



Optics Letters

Multilevel phase-type diffractive lens embedded in sapphire

QIAN-KUN LI,¹ YI-MING LU,¹ JIAN-GUAN HUA,¹ YAN-HAO YU,¹ LEI WANG,¹  QI-DAI CHEN,^{1,*} SAULIUS JUODKAZIS,^{1,2,3}  AND HONG-BO SUN¹

¹State Key Laboratory on Integrated Optoelectronics, College of Electronic Science and Engineering, Jilin University, Changchun 130012, China

²Centre for Micro-Photonics, Faculty of Science, Engineering and Technology, Swinburne University of Technology, Hawthorn, VIC 3122, Australia

³Melbourne Centre for Nanofabrication, ANFF, 151 Wellington Road, Clayton, VIC 3168, Australia

*Corresponding author: chenqd@jlu.edu.cn

Received 25 July 2017; revised 20 August 2017; accepted 30 August 2017; posted 31 August 2017 (Doc. ID 302048); published 22 September 2017

Herein, we report a kinoform phase-type lens (KPL), which is fabricated by femtosecond (fs)-laser-induced refractive index change inside sapphire crystal. By fabricating volume phase gratings in sapphire and measuring the energy ratio of the grating's first and second diffraction orders, the refractive index change in sapphire induced by fs-laser modification was obtained. Then a four-level KPL was designed and fabricated inside sapphire following the experimentally established scaling of the refractive index change and fs-laser power. Importantly, the KPL has unique UV focusing and imaging capability as well as a stable optical performance in different refractive index environments. The KPL embedded in sapphire has the same optical performance after a high-temperature (1050°C) annealing for 30 min. The KPLs in sapphire have great potential to increase light extraction efficiency in GaN blue-UV light-emitting diodes and can be used in micro-optical sensor applications in chemically harsh and high-temperature environments. © 2017 Optical Society of America

OCIS codes: (230.3990) Micro-optical devices; (350.3390) Laser materials processing; (050.7330) Volume gratings; (220.4000) Microstructure fabrication.

<https://doi.org/10.1364/OL.42.003832>

Recently, femtosecond (fs) laser direct writing (FsLDW) has become a popular method to fabricate three-dimensional (3D) optical structures in various transparent materials by laser-induced refractive index change or form birefringence due to nano-gratings in glass [1–7]. Also, planar 2D optical elements can be created, e.g., graphene oxide can be reduced by a focused fs-pulsed laser exposure to form micro-lenses [1]. FsLDW was used to inscribe Bragg grating sensors in silica fiber for temperature/pressure sensors [2]. Similarly, waveguides in glass can be written for applications in quantum optics, and optical lanterns in astro-physics [3,4]. Polymer- and protein-based micro/nanoscale structures could be successfully fabricated by FsLDW technique for soft micro-optics and

bio-implantable devices [5]. Complex optically chiral structure and volumetric aperiodic patterns were demonstrated with fs-laser irradiation [6,7]. It is well known that sapphire's optical and mechanical properties could be modified by focused fs-laser pulses [8]. Most of the reported results related to laser processing of sapphire had a focus on the fundamental light-material interaction, namely, the study of surface ablation [9], crystal-line-amorphous state transition [10], surface and in-bulk structuring [11], and laser-induced damage threshold [12]. Surface processing of sapphire was demonstrated for optical and sensor applications [13]. However, as one of the most widely used materials in optics and optoelectronic applications, sapphire is still not sufficiently exploited for fabrication of micro-optical devices by fs-laser-induced refractive index change. Obviously, micro-optical elements embedded inside material have distinct advantages compared with surface optical elements. First, the internal structures are not easily broken or covered with accidental particulates, and they can perform in environments with changing conditions (refractive index).

In this study, we investigated a fs-laser-induced refractive index change of sapphire for fabrication of a highly efficient micro-diffractive optical element—a kinoform phase lens (KPL)—inside sapphire by FsLDW. First, volume phase gratings were made by laser-induced refractive index change to quantify the refractive index change by measuring the energy ratio of the diffraction orders. With the measured value of refractive index change, we have designed and fabricated multilevel phase-type diffractive lenses inside sapphire and tested their performance at UV spectral range. Also, optical performance of the lenses in different refractive index environments and after high-temperature (1050°C) heat treatment was studied.

In experiments, a high numerical aperture (NA = 0.45 and magnification 40×) UV reflection-type objective lens (LMM-40X-UVV, Thorlabs) was used to tightly focus fs-laser pulses to process a 430- μm -thick c-plane sapphire crystal. Laser pulses generated by the fs-laser amplifier (Pharos, Light Conversion) had 290 fs pulse duration and 343 nm wavelength and were used at 200 kHz repetition rate. The shorter the wavelength, the smaller the nonlinear effects related to the white-light

continuum and self-focusing [14]. Pulse energy was measured at the entrance of the objective lens. A fast laser beam scanning speed can be used at the 200 kHz laser repetition rate to improve fabrication throughput and, at the same time, not to cause a strong heat accumulation that could facilitate crack formation [15]. For fabrication of 3D KPL patterns, the complex 3D geometry of a micro-lens was first designed in C# language and then converted into computer processing data for beam 3D scanning. The beam's vertical movement was controlled by a piezo stage with a 1 nm precision (PI P-622 ZCD). Simultaneously, a two-galvano-mirror set was used to control the sample's horizontal exposure during beam scanning. A circularly polarized laser beam was generated using a quarter-wave plate in order to avoid artifacts caused by a linear laser polarization, which produces a different thermal accumulation when scanning direction is changed [12,16].

Schematics of the fs-laser 3D direct writing is shown in Fig. 1(a). Tightly focused fs-laser pulses at the dielectric breakdown conditions modified sapphire via multi-photon and avalanche absorption with low propensity of micro-crack formation due to high Young modulus of the host [8,17]. By precisely optimizing laser power and scanning speed, the laser-modified region can be sustained without cracks inside the sapphire. Thus, FsLDW can inscribe arbitral 3D-designed patterns and complicated structures with a nanometric precision in the placement of modification [17,18]. The refractive index of the laser-modified region, n' , is different from the index, n , of the host sapphire crystal. Actually, the change of refractive index in the fs-laser-modified region has a gradient. Here, we assume that the refractive index of the fs-laser modification region is homogeneous. When light is transmitted through the area modified by the fs-laser, the phase is modulated; the absorption losses were insignificant for the visible wavelengths. The phase difference is defined by the product of the length and the refractive index change. Hence, a measurement of the refractive index change, Δn , has a practical significance for precise design of the retardance. Figure 1(b) shows the diffraction of the HeNe laser beam (632.8 nm) from a volume phase grating. By measuring the energy distribution of the diffracted light, the phase change is obtained and, for the known grating depth, the refractive index change is quantified. In the case of the volume phase grating, the efficiency of the m -th diffraction order, η_m , is given by [19]

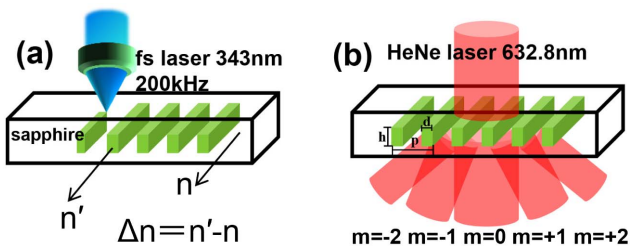


Fig. 1. (a) Schematics of a fs-laser 3D direct writing; n is the refractive index of the sapphire, and n' is the refractive index of the laser-modified region. (b) Sketch of a volume phase grating diffracting a HeNe laser beam of 632.8 nm wavelength; h , p , and d are the height, period, and width of laser-modified regions, respectively; m is the diffraction order.

$$\begin{cases} \eta_0 = 1 - 2\rho(1 - \rho)(1 - \cos \Delta\phi) \\ \eta_{m \geq 1} = \frac{1}{m^2 \pi^2} (1 - \cos 2m\pi\rho)(1 - \cos \Delta\phi) \end{cases}, \quad (1)$$

where ρ is the duty ratio of volume phase rectangular grating, and $\Delta\phi$ is the phase delay of light. Equation (1) shows that the energy of each diffraction order depends on ρ and $\Delta\phi$. According to the theory of scalar diffraction [19], the phase delay $\Delta\phi$ is given by

$$\Delta\phi = \frac{2\pi\Delta n h}{\lambda}, \quad (2)$$

where Δn is the refractive index difference between the laser-modified region and sapphire host, and h is the depth of the grating. Equation (2) determines the relation between the phase change $\Delta\phi$ and Δn and h . By measuring energy distribution of the diffraction orders for the known duty ratio and depth of the grating (a side-view optical observation), the refractive index change was obtained.

An image of the fabricated volume phase grating embedded in sapphire crystal is shown in Fig. 2(a); the period of the grating was 5 μm , and the region that appears brighter was inscribed by fs-laser exposure. The width of the fs-laser modified region is approximately 1 μm , hence, the duty ratio ρ of the grating is 1:5. Figure 2(b) shows the cross-sectional side-view image of the volume phase grating fabricated inside sapphire.

The depth of the volume phase rectangle grating was 6.3 μm . The side of the sapphire sample was polished using fine sandpaper for observation. The diffraction orders of the

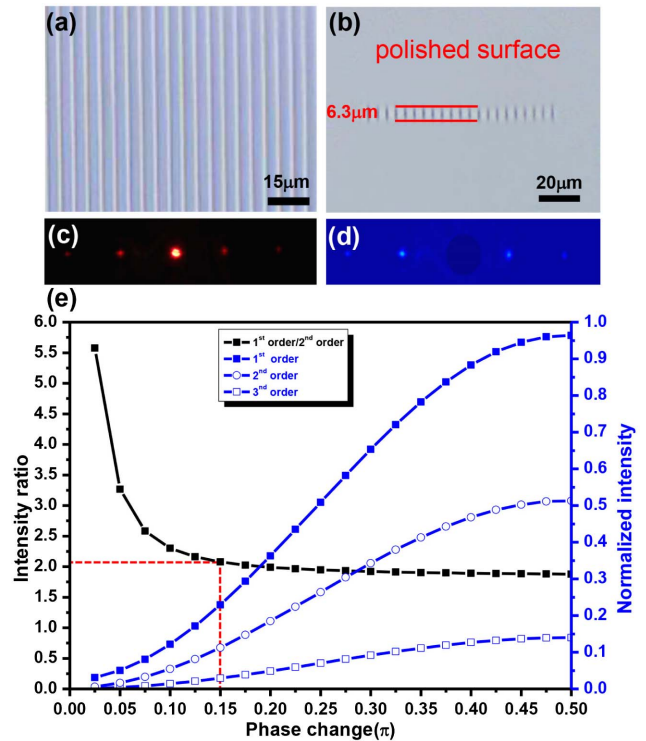


Fig. 2. (a) Optical microscope image of the volume phase grating fabricated inside sapphire. (b) Side-view image of the volume phase grating in sapphire. (c) Optical photographs of grating's diffraction patterns; 0-th order blocked for numerical estimation of the diffraction efficiencies. (d) Energy of diffraction orders extracted via image [shown in (c)] processing. (e) Theoretical calculation of the energy of different orders and the phase change. The duty ratio is 1:5.

volume phase grating were investigated under HeNe laser illumination at a power of 120 mW. The diffraction pattern of the grating is shown in Fig. 2(c), which was taken by an optical camera behind the sample. The intensities of the zero, first, and second diffraction orders were measured, respectively. Figure 2(d) is the digitized image of the panel (c) using MATLAB with the 0-order spot eliminated due to saturation. The precise energy ratio of the first and second diffraction orders was 2.01 [Fig. 2(d)]. The theoretical normalized diffracted powers were simulated by optical wave propagation based on the Fresnel diffraction theory and are shown in (e). The normalized diffraction intensities of the first, second, and third diffraction orders relative to the phase change are plotted together with the energy ratio between the one to two orders. By comparison of the measured experimental data and the theoretical value, the phase retardance of 0.15π was obtained. From Eq. (2) and the measured depth of grating $h = 6.3\ \mu\text{m}$, the refractive index change $\Delta n = 7.53 \times 10^{-3}$ is obtained. This value has an important guiding significance for the design and fabrication of high efficiency KPL and other optical devices. The maximum laser power at which the largest refractive index change was achieved without micro-crack formation at the used focusing conditions was $7.7\ \mu\text{J}/\text{pulse}$. It was used to write KPLs that have minimal light scattering and are mechanically stable.

Shown in Figs. 3(a) and 3(b) are the front and side views of the inscribed four-level phase-type diffractive lens embedded in sapphire crystal host. The innermost radius of the fabricated lens was $10\ \mu\text{m}$, and the theoretical design wavelength and focal length were $365\ \text{nm}$ and $274\ \mu\text{m}$, respectively. For this KPL phase-type lens, both the odd and even number zones are transparent. A pair of the even-odd number zones is divided into a series of subzones with sequentially varied thicknesses. For N -level KPL, the efficiency is determined by [20]

$$\eta(N) = \frac{\sin^2(\pi/N)}{(\pi/N)^2} = \sin^2(1/N). \quad (3)$$

For $N = 2$ and $N = 4$, theoretical efficiencies are 40.5% and 81.0%, respectively. Experimentally, the phase modulation of the diffractive lens was realized by thickness variation in subzones. For N -level KPL, its thickness is defined by $h = \lambda/N \times \Delta n$; hence, for the four levels at $365\ \text{nm}$ wavelength, the single level thickness is $12.12\ \mu\text{m}$ in order to induce the phase modulation of π . Figure 3(b) shows that the thickness of subzones is about $12\ \mu\text{m}$, which is slightly smaller than the required theoretical value. Precision of the axial extent of the focal region is strongly affected by spherical aberration (depth of the focal laser writing position) and self-focusing [21]. However, due to a threshold effect of modification and a short laser wavelength, a high precision of inscription in sapphire was feasible [Fig. 2(b)].

The UV beam focusing and imaging performance of the fabricated KPL embedded in sapphire are shown in Figs. 3(c) and 3(d). The experimentally measured focal length of the KPL was $279\ \mu\text{m}$, which is comparable to the theoretically designed value of $274\ \mu\text{m}$ at $365\ \text{nm}$ wavelength. The measured diffractive efficiency of KPL, defined as the ratio of the energy collected at the prime focus to the total incident power was 70.5%, which was slightly smaller than the theoretical diffraction efficiency of 81.0% for the four-level KPL. The thickness of the diffractive lens embedded in sapphire is a few tens of micrometers, and the laser-induced refractive index changes

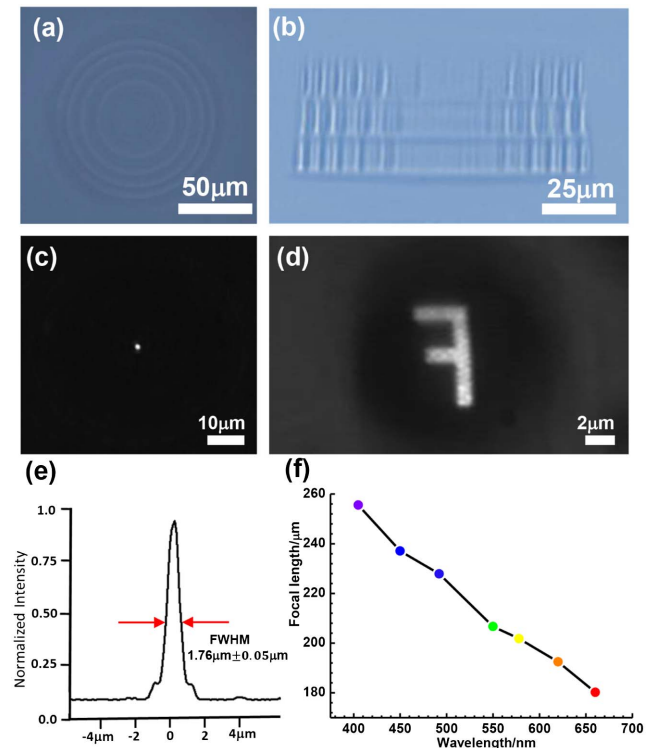


Fig. 3. (a) Optical microscope image of four-level phase-type diffractive lenses fabricated inside sapphire. (b) Side-view image of four-level phase-type diffractive lenses fabricated inside sapphire. (c) UV focusing characteristics of the lens at $365\ \text{nm}$ wavelength. (d) UV imaging performance of the four-level phase-type diffractive lenses fabricated inside sapphire. (e) Normalized intensity cross section of the focal spot. (f) Focal length of KPL at different wavelengths.

were slightly different along the depth of writing, as discussed above. This accounts for the discrepancy between the measured and theoretical efficiencies. Efficiency obtained here is much higher than those reported by other fs-laser writing experiments [22]. Figure 3(d) shows KPL's clear imaging performance at UV wavelength, i.e., an image of the capital letter "F" is obtained with good quality. The diffractive lens also produces a clear, well-defined focal spot of $r = 1.76\ \mu\text{m} \pm 0.05\ \mu\text{m}$ [full width at half-maximum, FWHM; Fig. 3(e)]. This focal spot size is comparable to the estimation of the focal spot that can be achieved by an ideal Fresnel lens, $r_{\text{FZP}} = 1.22 \times \Delta r \approx 1.78\ \mu\text{m}$, where Δr is the smallest zone width. By plotting the measured focal length for different wavelengths of a monochromatic incident light, a typical tendency expected for the chromatic dispersion is revealed in Fig. 3(f). The focal length decreased from $255\ \mu\text{m}$ to $180\ \mu\text{m}$ by tuning the wavelength from $405\ \text{nm}$ to $660\ \text{nm}$. The KPL in sapphire exhibits excellent UV focusing and imaging virtues, which have great importance in the field of UV LED because sapphire is one of the most widely used substrate materials for GaN LEDs.

For the phase-type diffraction optical element made on a surface, the external refractive index of the ambience has a significant effect on the diffraction efficiency. For the KPL formed inside a host dielectric matrix, the influence of the ambient environment on optical performance is eliminated. The independent optical properties of the KPL in different refractive index environments were tested by imaging. Figures 4(a)

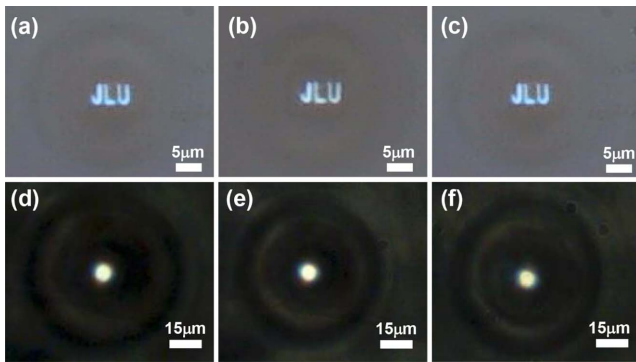


Fig. 4. Imaging and focusing properties under white-light performance in different environments. Imaging of the letters JLU in: (a) air and (b) water. (c) Imaging in air after a high-temperature (1050°C) annealing for 30 min. The focal spot at the focal plane in: (d) air, (e) water, and (f) after high-temperature annealing of the KPL.

and 4(d) show imaging and focusing of visible light in air, while Figs. 4(b) and 4(e) show the same with the sample placed inside a cuvette filled with water. It is obvious that optical properties of the KPL made in sapphire had no performance change, regardless of the ambient refractive index. KPL is buried below the surface (inside) sapphire, and the phase modulation defined by the KPL structure governs its optical performance and images inside different external refractive index environments.

The temperature to grow GaN LEDs on sapphire substrate is 1050°C [23]. Since the optical elements and structures for light extraction from LEDs can be made on/in sapphire substrate before high-temperature growth of LEDs [24], it is necessary to measure performance of KPL inscribed in sapphire under the high-temperature treatment. Figures 4(c) and 4(f) show optical performance of the KPL after annealing at 1050°C for 30 min and compared to the performance before heat treatment. No degradation of optical performance was observed, which makes such KPL in sapphire useful for applications in high-efficiency GaN blue UV LEDs and for optical sensors in harsh and high-temperature industrial applications.

In summary, a high-efficiency ($\sim 71\%$) multilevel phase-type diffractive lens embedded in sapphire has been fabricated by fs-laser-induced refractive index change. The conditions of $\Delta n = 7.53 \times 10^{-3}$ were chosen for lens recording, since there were no micro-cracks formation with minimal scattering and absorbance changes in transmission. In this work, the refractive index change induced by fs-laser writing was measured first from inscribed volume phase gratings inside sapphire by calculating the ratio of diffracted energy between first and second orders for the directly measured axial extent of the laser-modified regions obtained by side-view imaging. With the accurate refractive index change established, efficient optical elements were designed and fabricated using flat-2D and volumetric-3D multilayer patterning inside sapphire.

The as-formed diffractive lens in sapphire showed excellent UV focusing and imaging performance, promising high-efficiency GaN blue UV LED applications. Lastly, the KPL in sapphire can keep stable optical performance in different

refractive index environments and can be used in high-temperature conditions. All of these merits give such a diffractive lens in sapphire great potential for practical applications as an outstanding UV micro-optical element, e.g., for lens arrays in sapphire for high-brightness GaN blue UV LEDs.

Funding. National Key R&D Program of China (2017YFB1104600); National Natural Science Foundation of China (NSFC) (61137001, 61435005, 61590930, 91323301, 91423102).

Acknowledgment. S. J. is grateful for the ChangJiang visiting scholar project at Jilin University.

REFERENCES

- X. Li, H. Ren, X. Chen, J. Liu, Q. Li, C. Li, G. Xue, J. Jia, L. Cao, A. Sahu, B. Hu, Y. Wang, G. Jin, and M. Gu, *Nat. Commun.* **6**, 6984 (2015).
- S. Derevyanko, *Opt. Lett.* **33**, 2404 (2008).
- L. Fan, C. L. Zou, M. Poot, R. Cheng, X. Guo, X. Han, and H. X. Tang, *Nat. Photonics* **10**, 766 (2016).
- F. Flamini, L. Magrini, A. S. Rab, N. Spagnolo, V. D'Ambrosio, P. Mataloni, F. Sciarrino, T. Zandrini, A. Crespi, R. Ramponi, and R. Osellame, *Light Sci. Appl.* **4**, e354 (2015).
- Y. L. Zhang, Q. D. Chen, H. Xia, and H. B. Sun, *Nano Today* **5**(5), 435 (2010).
- B. Pommellec, M. Lancry, R. Desmarchelier, E. Hervé, and B. Bourguignon, *Light Sci. Appl.* **5**, e16178 (2016).
- T. D. Gerke and R. Piestun, *Nat. Photonics* **4**, 188 (2010).
- S. Juodkakis, K. Nishimura, H. Misawa, T. Ebisui, R. Waki, S. Matsuo, and T. Okada, *Adv. Mater.* **18**, 1361 (2006).
- C. W. Chang, C. Y. Chen, T. L. Chang, C. J. Ting, C. P. Wang, and C. P. Chou, *Appl. Phys. A* **109**, 441 (2012).
- V. Mizeikis, S. Kimura, N. V. Surovtsev, V. Jarutis, A. Saito, H. Misawa, and S. Juodkakis, *Appl. Surf. Sci.* **255**, 9745 (2009).
- A. Vaillonis, E. G. Gamaly, V. Mizeikis, W. Yang, A. V. Rode, and S. Juodkakis, *Nat. Commun.* **2**, 445 (2011).
- O. Uteza, B. Bussiere, F. Canova, J. P. Chambaret, P. Delaporte, T. Itina, and M. Sentis, *Appl. Surf. Sci.* **254**, 799 (2007).
- R. Buividas, P. R. Stoddar, and S. Juodkakis, *Ann. Phys. (Berlin)* **524**, L5 (2012).
- O. M. Efimov, K. Gabel, S. V. Garnov, L. B. Glebov, S. Grantham, M. Richardson, and M. J. Soileau, *J. Opt. Soc. Am. B* **15**, 193 (1998).
- S. M. Eaton, H. Zhang, M. L. Ng, J. Li, W. J. Chen, S. Ho, and P. R. Herman, *Opt. Express* **16**, 9443 (2008).
- V. Stankevič, G. Račiukaitis, F. Bragheri, X. Wang, E. G. Gamaly, R. Osellame, and S. Juodkakis, *Sci. Rep.* **7**, 39989 (2017).
- K. Sugioka and Y. Cheng, *Light Sci. Appl.* **3**, e149 (2014).
- M. Malinauskas, A. Žukauskas, S. Hasegawa, Y. Hayasaki, V. Mizeikis, R. Buividas, and S. Juodkakis, *Light Sci. Appl.* **5**, e16133 (2016).
- J. B. Marion and M. A. Heald, *Classical Electromagnetic Radiation* (Elsevier, 1965), p. 368.
- Q. D. Chen, D. Wu, L. G. Niu, J. Wang, X. F. Lin, H. Xia, and H. B. Sun, *Appl. Phys. Lett.* **91**, 171105 (2007).
- R. G. Rafael and M. Eric, *Nat. Photonics* **2**, 219 (2008).
- W. Watanabe, D. Kuroda, and K. Itoh, *Opt. Express* **10**, 978 (2002).
- D. Y. Kim, J. H. Park, J. W. Lee, S. Hwang, S. J. Oh, J. Kim, C. Sone, E. F. Schubert, and J. K. Kim, *Light Sci. Appl.* **4**, e263 (2015).
- T. Kudrius, G. Šlekys, and S. Juodkakis, *J. Phys. D* **43**, 145501 (2010).